Comparative Analysis of Cycle-to-Cycle Variabilities and Combustion Development in an Optical Spark-Ignition Engine Fueled by Pure Hydrogen and Propane: Insights from Chemiluminescence and PIV

Caio Ramalho Leite, Pierre Brequigny, Jacques Borée, Fabrice Foucher

Comparative Analysis of Cycle-to-Cycle Variabilities and Combustion Development in an Optical Spark-Ignition Engine Fueled by Pure Hydrogen and Propane: Insights from Chemiluminescence and PIV

C. Ramalho Leite[1,*], P. Brequigny[1], J. Borée[2], F. Foucher[1]

1: Université d'Orléans, INSA CVL, Laboratoire Prisme – EA 4229, F-45072 Orléans, France
2: Departement Fluides Thermiques et Combustion, Institut Pprime – UPR 3346, CNRS-ENSMA – Université de Poitiers, 86360 Futuroscope-Chasseneuil, France
* Correspondent author: caio.rleite@univ-orleans.fr

Keywords: Ultra-lean hydrogen flames, In-cylinder aerodynamics, Cyclic variability, PIV, Chemiluminescence

ABSTRACT

Hydrogen, derived from renewable sources and devoid of carbon emissions, is a pivotal energy carrier for the future. Representing a viable substitute for fossil fuels in internal combustion engines (ICEs), contemporary studies advocate using very-lean and ultra-lean hydrogen-air mixtures, with a fuel-air equivalence ratio below 0.5, as a potent strategy to reduce NOx emissions in hydrogen-fueled ICEs. An experimental setup with an optical spark-ignition engine was devised to investigate the primary factors influencing cycle-to-cycle variations in H2ICEs by optimizing mixture homogeneity and focusing the study on flame interaction with in-cylinder aerodynamics. Simultaneous in-cylinder pressure, chemiluminescence, and PIV analyses were performed to characterize and compare the behaviors of ultra-lean hydrogen-air and propane-air flames, assessing flame development and cyclic variation features. Results indicate that the flame development of hydrogen and propane is significantly different. Propane exhibited increased in-cylinder pressure trace variability at lean and rich flammability limits with a high flame development difference between fast and slow cycles. In contrast, hydrogen-air mixtures under various equivalence ratios (from very-lean to ultra-lean) presented much more stable in-cylinder pressures. Furthermore, fast propane flames were mainly advected to the cylinder's symmetrical axes, while fast hydrogen flames started further away from the spark plug. Horizontal and vertical PIV measurements showed a single structure flow field over the studied conditions with mainly intensity variations over the measured cycles. Fast flames were associated with more intense tumble motion. The differences between fast and slow flames for hydrogen are attributed to the early flame development. However, after initial differences in flame development over several crank angles, there are similarities in all cycles, suggesting that the low variability in in-cylinder pressures is mostly due to the robustness of hydrogen flame ignition and its independence from in-cylinder flow small variations at the early development phase.

1. Introduction

Hydrogen, derived from renewable sources and devoid of carbon emissions, is a pivotal energy carrier for the future. Representing a viable substitute for fossil fuels in internal combustion engines (ICEs), hydrogen not only holds the promise of zero-carbon emissions but also signifies a pathway

to geopolitical autonomy regarding energy and material supply (Lebrouhi et al., 2022; Verhelst & Wallner, 2009). Contemporary studies advocate using very-lean and ultra-lean hydrogen-air mixtures, with a fuel-air equivalence ratio below 0.5, as an effective strategy to reduce NOx emissions in hydrogen-fueled ICEs (H2ICEs) (Ramalho Leite, Oung, et al., 2023).

While lean mixtures are known for causing higher operational instability and increased cycle-to-cycle variations (CCVs) (Truffin et al., 2015), the distinctive characteristics of hydrogen flames - including a wide flammability range, lower minimum ignition energy, and unique transport phenomena - suggest different behaviors. Hydrogen-air flames, particularly in low equivalence ratio mixtures and high pressures, exhibit thermodiffusive instabilities (Berger et al., 2022; Chu, Berger, Grenga, Gauding, et al., 2023; Chu, Berger, Grenga, Wu, et al., 2023; Ramalho Leite, Laignel, et al., 2023). These instabilities are proven to accelerate the combustion process, leading to significant modifications in flame development and potentially impacting its variability in ICE conditions (Ramalho Leite, Oung, et al., 2023).

Extensive research has been conducted to assess the impacts of various parameters on engine stability (Ding et al., 2023; Enaux et al., 2011; Truffin et al., 2015). However, physical analyses of the underlying mechanisms are still needed. This is particularly important for explaining the distinctions between ultra-lean hydrogen and other conventional fuels regarding flame development and fluctuation behavior in conditions representative of in-cylinder turbulent flows.

The present study aims to characterize the distinct behaviors of homogeneous ultra-lean hydrogen-air flames and propane-air flames, focusing on flame development and cyclic variations. To achieve this, the following analyses are conducted:

1. Comparing in-cylinder pressure traces for pure hydrogen and propane under similar load conditions.
2. Characterizing the internal aerodynamics of the optical engine through the Empirical Mode Decomposition.
3. Characterizing the flames of both fuels using chemiluminescence imaging across multiple equivalence ratios at the same thermodynamic conditions.
4. Highlighting flame features and comparing fast and slow cycles for each fuel.
5. Understanding the impact of aerodynamics on hydrogen flame variability through PIV measurements.

The data presented in this work aims to enrich the database on ultra-lean hydrogen-fueled internal combustion engines with homogeneous mixtures and highlight the effect of the fundamental properties of hydrogen-air flames within an engine. This research can help the development of hydrogen combustion simulations in both 0D/1D and CFD by distinguishing the complexity of mixing from that of the flame itself.

2. Experimental setup and methodology

An experimental setup was devised to investigate the primary factors influencing CCV in H2ICEs. The experimental bench prioritizes optimizing mixture homogeneity, focusing the study on flame interaction with in-cylinder aerodynamics and assessing the combustion features of hydrogen-air mixtures compared to a well-known fuel.

Experiments were conducted using a single-cylinder optical spark ignition engine, specifically the PSA EP6 model, featuring a Bowditch piston design, displayed in Figure 1. This engine has a displacement of 0.4 liters and a compression ratio of 9.5. The cylinder head is of the pent-roof type, and the engine has an optical piston bowl with 41 mm of diameter. Hydrogen or propane injection was performed continuously, positioned 700 mm upstream of the intake valves, with studies validating the achievement of homogeneous mixture distribution within the combustion chamber [XXX].

During all experiments, the intake air was dehumidified and filtered, with its flow regulated by an Emerson Micro Motion F025S Coriolis flow meter, accurate to 0.5% of the flow rate. Hydrogen flow was managed and monitored using a 30 NLPM Brooks 5850S mass flow meter with a 0.2% full-scale accuracy.

Additionally, the cooling water and oil were consistently maintained at 85°C. Intake and exhaust temperatures were monitored using K-type thermocouples in both plenums and pipes. Pressure measurements were taken at locations 200 mm and 160 mm away from the intake and exhaust valves, respectively. Kistler 4075A piezoresistive sensors, with a 0.1% full-scale accuracy, were used for pressure measurements. In-cylinder pressure was measured using an AVL QH32C piezoelectric transducer, with a 0.2% full-scale accuracy.

The engine is connected to an electric motor, allowing for motoring conditions between 600 and 1900 rpm. Data is recorded at intervals of 0.1 crank angle degrees using an optical encoder (Kubler 5020). All parameters are managed and stored using a custom LabView control system.

A preliminary investigation was undertaken using a pressure-based analysis to assess engine stability across 100 consecutive cycles using both fuels. The equivalence ratio was adjusted to maintain a constant indicated mean effective pressure (IMEP) of 3 bar, while intake pressure and spark timing were adjusted to achieve the desired load at optimal combustion timing. This condition is chosen because higher CCVs are found at low load conditions and intake pressure was limited to 0.4 bar at 1200 rpm by the air mass flow controller, a condition which is found with stoichiometric propane for 3 bars of IMEP. Then, to analyze and compare the propagation of the flames under various conditions, the spark timing is set at -15 degrees after the Top Dead Center (°aTDC), ensuring similar thermodynamic conditions at the onset of the flame kernel.

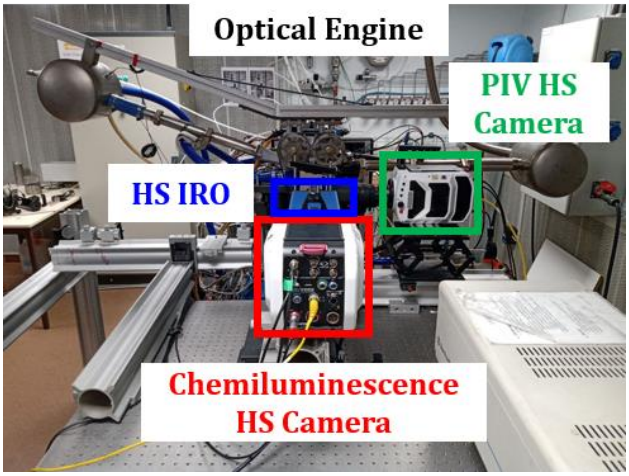

Figure. 1 Experimental test bench with the simultaneous PIV and chemiluminescence setup.

1. *Horizontal Chemiluminescence Imaging*

Chemiluminescence measurements are conducted concurrently with in-cylinder pressure using the Bowditch piston. Images are captured using a high-speed camera (Phantom v1610) coupled with a high-speed intensifier (La Vision High-speed IRO), a UV-sensitive objective lens of 100 mm, and a Newport UG5 band-pass filter (center wavelength of 318 nm and full width at half-maximum of 175 nm).

For the chemiluminescence analysis, the image magnification factor is 0.092 mm per pixel, with the imaging frequency adjusted to capture a flame image at every crank angle degree. Initially, the

intensifier gain and gate settings are configured at 50% and 30 µs, respectively, at an equivalence ratio of 0.55. These settings are gradually increased to 70% and 80 µs at an equivalence ratio of 0.20. Subsequently, the images undergo post-processing, which involves several steps: applying a median filter (7x7 pixels), binarization (with a threshold varying from 10 to 20% of the image's maximum pixel intensity depending on the equivalence ratio), and contour detection.

Various parameters are extracted, including the projected surface area and the equivalent flame radius. This analysis is conducted throughout the engine cycle, from -15° to +16 °aTDC, ending when the flame contour exceeds the piston window boundary. Another significant parameter that can be computed is the equivalent flame propagation speed, defined as the change in the equivalent flame surface radius over the time interval between two crank angles. Statistics are calculated over 100 cycles, and the mean values are considered valid if there are more than 50 cycles at a given crank angle.

2. Horizontal PIV Measurements

Particle Image Velocimetry (PIV) experiments are conducted using a high-speed 532 nm Nd:YAG laser (Quantronix Dual Hawk-HP). A laser sheet is generated with a thickness of approximately 1 mm and positioned 5 mm below the center electrode of the spark plug in the xy plane, as shown in Figure 2. Velocity fields were measured from 195 to 30 °bTDC at every 5 crank angles. Silicon oil droplets (d_p ≈ 1 µm) were seeded upstream of the intake plenum, and the time between frames was set to 25 µs.

The velocity fields are obtained using DaVis software. The field of view measures 22x40 mm^2, and the pixel size is 0.052 mm. Image pre-processing includes contrast-limited adaptive histogram

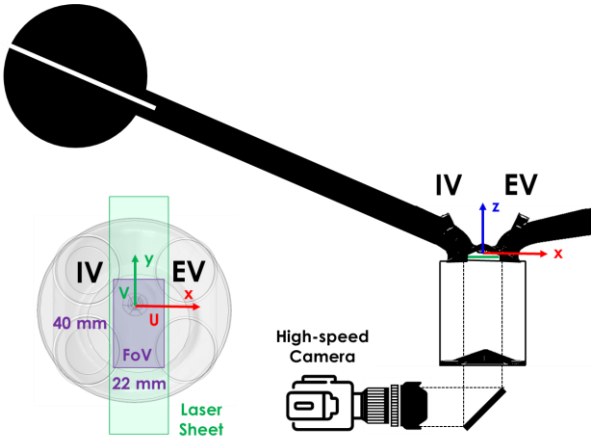

Figure. 2 Schematics of the horizontal PIV setup.

equalization (CLAHE) of 64x64 pixels² and background subtraction (using the mean intensity). PIV calculations are performed with two passes in an interrogation area of 32x32 pixels² with 50% overlap. The final vectors are defined at every 0.82x0.82 mm². Finally, image-based low and high contrast filters of 0.1% and 50%, respectively, are applied, along with a vector-based standard deviation filter of 8σ and a local median filter of 3.

Two decomposition methods are employed to analyze the PIV fields: 1) the Reynolds Decomposition and 2) the Empirical Mode Decomposition (EMD).

The Reynolds Decomposition separates the instantaneous velocity field, $\boldsymbol{U}$, into an ensemble average component, $\langle \boldsymbol{U} \rangle$, and a fluctuating component, $\boldsymbol{u}$, as shown in the equation below. This decomposition enables the examination of the primary flow field pattern and the in-cylinder turbulence intensity and flow variability across different configurations as a function of crank angle. The variation in the flow field can be quantified by the root mean square of the fluctuating component, denoted here as $\boldsymbol{u}'$.

$$\boldsymbol{U} = \langle \boldsymbol{U} \rangle + \boldsymbol{u}$$

The second method decomposes the velocity field in a low-frequency component, U_{LF}, and a high-frequency component, u_{HF} (Sadeghi et al., 2019). This approach provides a more precise characterization of the high-frequency component, as the fluctuating velocity in the previous decomposition stems from the variability of both high-frequency and low-frequency components. Consequently, variations attributable to the high-frequency component are typically associated with turbulence, while variability in the low-frequency flow field is linked to engine cycle-to-cycle variations (CCV) (Ding et al., 2023).

$$\boldsymbol{U} = \boldsymbol{U_{LF}} + \boldsymbol{u_{HF}}$$

Consequently, the ULF component can be divided into an ensemble average component, $\langle \boldsymbol{U_{LF}} \rangle$, and the cyclic variations component, $\boldsymbol{u_{CCV}}$.

$$\boldsymbol{U_{LF}} = \langle \boldsymbol{U_{LF}} \rangle + \boldsymbol{u_{CCV}}$$

The EMD decomposition for a given cycle and CAD is shown in Figure 3.

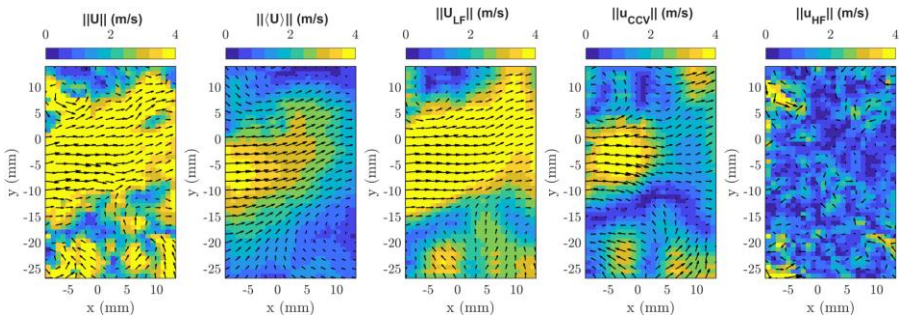

Figure. 3 Empirical Mode Decomposition (EMD) velocity fields at 35 ◦bTDC.

3. Vertical Simultaneous Chemiluminescence and PIV

A second high-speed camera (Phantom v1611) and a short-pass dichroic mirror (Transmission: 300 - 350 nm, Reflection: Visible wavelengths) are integrated to facilitate simultaneous chemiluminescence and PIV measurements. The high-speed camera, connected to the high-speed Intensifier and UV filter, is directed towards the quartz window optical access at the cylinder head to visualize the flame near the spark plug. Meanwhile, the high-speed v1611 camera, equipped with a 200 mm objective lens and a band-pass filter (CWL: 532 nm; FWHM: 10 nm), is positioned to capture PIV measurements, with the dichroic mirror set at a 45-degree angle between the Intensifier and the quartz window. The schematics of the vertical PIV and chemiluminescence imaging are illustrated in Figures 4 and 5.

In both configurations, the pixel sizes are 0.094 mm/pixel and 0.044 mm/pixel, respectively, and images are captured at every 2 crank angle degrees from 90 °bTDC to 20 °aTDC. Post-processing analyses in the vertical plane are conducted similarly to those in the horizontal plane.

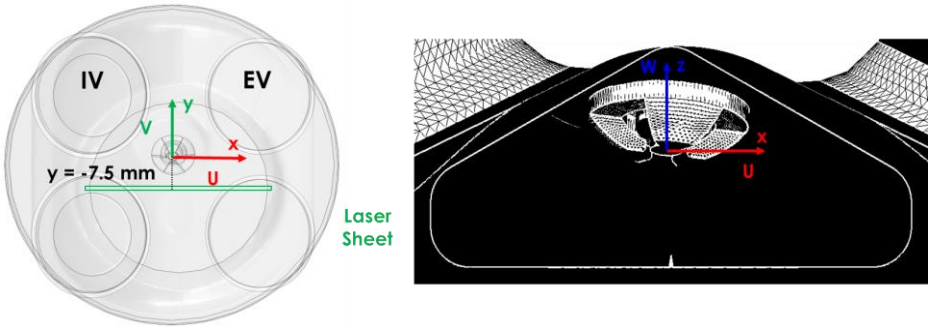

Figure. 4 Schematics of the vertical Chemiluminescence and PIV setups.

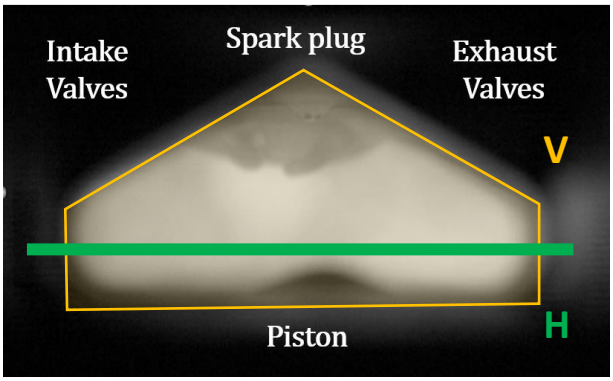

Figure. 5 Vertical optical window analysis scheme.

3. Results and Discussion

1. Differences between hydrogen and propane-fueled engines

The preliminary experiments revealed notable disparities in hydrogen and propane combustion behavior operating under identical loads. Particularly, distinct performances were observed in three combustion phases (0-10%, 10-50%, and 50-90% of burned mass fraction) across varying equivalence ratios, as depicted in Figure 6. With propane, a slight extension in combustion duration was noted as the mixture deviated from the equivalence ratio 1.1. This extension heightened cyclic variations and led to misfires at both ends of the equivalence ratio spectrum. Conversely, hydrogen variability exhibited less sensitivity, even with a more significant reduction in combustion speed under ultra-lean conditions. This suggests that factors beyond flame propagation speed contribute to the observed fluctuations.

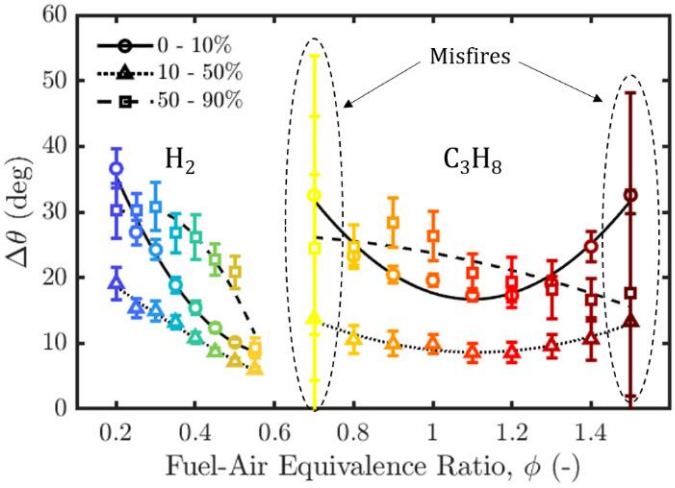

Figure. 6 Combustion duration of three combustion phases and their fluctuations as a function of the fuel-air equivalence ratio for hydrogen-air and propane-air mixtures under an IMEP of 3 bars. The error bars are relative to ±2σ.

2. *Internal aerodynamics characterization of the optical engine*

Initially, PIV was employed in a motoring case to capture cycle-resolved velocity fields near the spark plug (as inside the cylinder was previously studied by Sadeghi [XXX]) and to identify potential cycle-to-cycle variations in the in-cylinder flow. This analysis was conducted in two planes: the horizontal (H) at 5 mm below the center electrode of the spark plug and the vertical (V) at 7.5 mm away from the spark plug, as depicted in Figure 7.

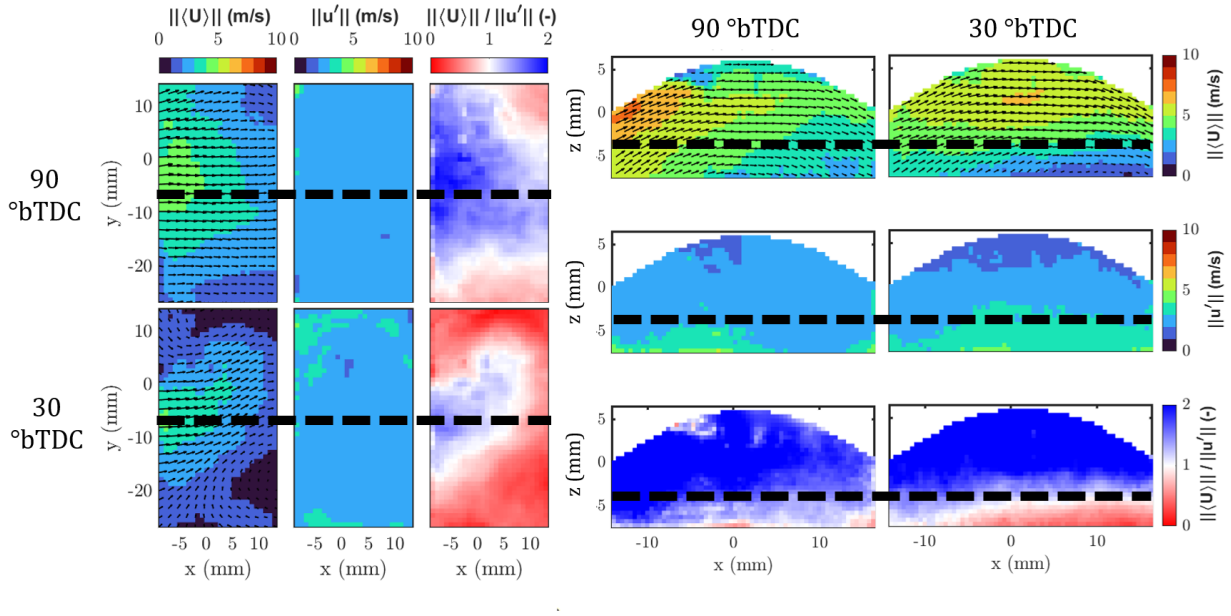

Figure. 7 Horizontal (left) and vertical (right) cold flow PIV under the same conditions (intake pressure of 0.7 bar and 1200 rpm) for 90 and 30 °bTDC. The black line shows the PIV plans.

The PIV measurements in both the horizontal and vertical planes at 90 °bTDC reveal a signature tumble motion, characterized by a quasi-symmetrical large-scale flow from the intake valves to the exhaust valves. The fluctuating velocity is quasi-isotropic across the domain. Given that the main flow velocity is around 5-6 m/s at this stage, the turbulent intensity is about 50% of the primary flow. By 30 °bTDC, however, the tumble structure appears to decelerate, with the mean flow deviating from the x direction and forming two vortexes centered at y = -20 mm and y = 10 mm. The fluctuating velocity now clearly dominates the flow.

Given the shared x-line in these two PIV measurements, a comparison is feasible. Consequently, the mean x component of velocity (U) and its standard deviation (u') are plotted at the same two

crank angles in Figure 8. The PIV measurements demonstrate consistency, revealing a mean U velocity of approximately 3-5 m/s at this x-line in both vertical and horizontal planes, with a standard deviation of 1-2 m/s at the midpoint of the compression stroke and 2-4 m/s at the end of the compression stroke, along with a u' of 2 m/s.

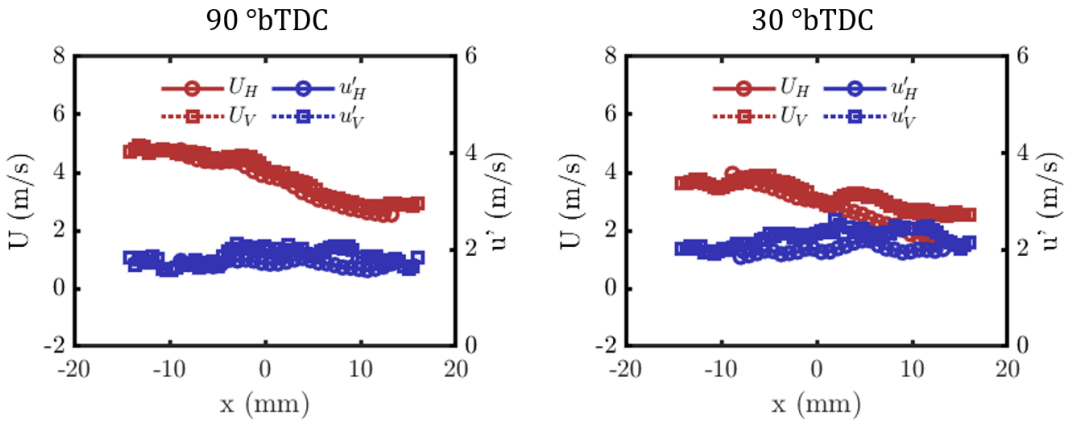

Figure. 8 Comparison of the mean velocity, U (in the x-direction), and its standard deviation, u', as a function of the x position on the PIVs planes' intersection line for the same 2 crank angles.

Figure 9 explores the kinetic energy associated with each velocity field component. Through EMD decomposition, the total kinetic energy of the field is divided into three parts: kinetic energy from the low-frequency component, kinetic energy from the high-frequency component, and the inner product of these two components (which is not zero). As shown in the figure, the low-frequency part of the flow contains the majority of the total kinetic energy, followed by the high-frequency component.

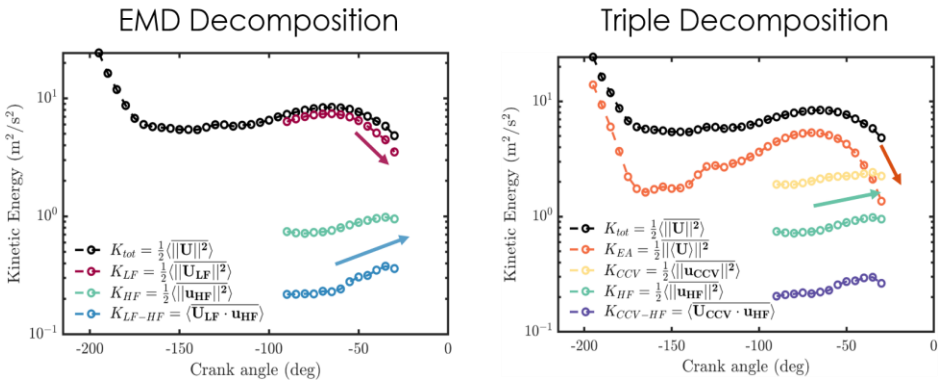

Figure. 9 Kinetic energy of each velocity component for the EMD decomposition (left) and the triple decomposition (right).

The triple decomposition is defined by dividing the low-frequency velocity field into the ensemble average (EA) and the fluctuations of the low-frequency flow (CCV). In the right graph of Figure 10, the amount of kinetic energy contributed by each component of the triple decomposition is shown. When compared to the left graph, it becomes clear that the low-frequency kinetic energy is split into the EA and CCV kinetic energies. The EA component follows the trend of the total kinetic energy but at lower values (approximately 60%). The CCV component exhibits higher kinetic energy than the high-frequency component, indicating that fluctuations in the large-scale structures have a greater impact on the energy than those in the small-scale structures.

Furthermore, Figure 10 illustrates the contribution of each velocity component to the total kinetic energy as a function of the crank angle. The low-frequency component of the velocity possesses the highest amount of kinetic energy, ranging from 80% to 90% at 90 °bTDC. This percentage begins to decrease at 60 °bTDC, eventually reaching 70% by 30 °bTDC. This analysis shows the tumble breakdown as the piston approaches TDC.

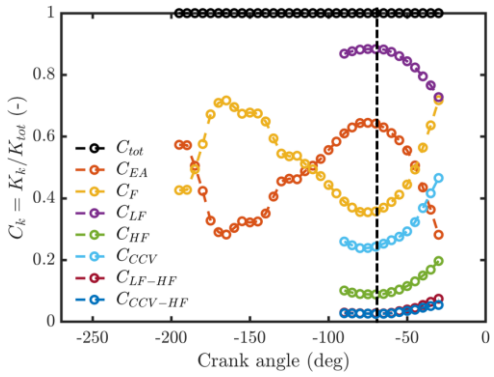

Figure. 10 Contribution of each velocity field kinetic energy to the total kinetic energy as a function of the crank angle.

The EA component shows a similar trend, with values around 60% at mid-compression, but the decrease in contribution is much more significant. Conversely, the general flow field fluctuation component (F), which complements the EA regarding the total kinetic energy, shows an opposite trend. This fluctuation is divided into the low-frequency part (CCV), the high-frequency part (HF), and the interaction between these two (CCV-HF). As previously stated, the CCV kinetic energy contributes more to the total kinetic energy and exhibits a stronger increase during the breakdown phase than the HF part.

3. In-cylinder pressure and flame development characterization

Further analysis was conducted by measuring the in-cylinder pressure and the chemiluminescence to elucidate the manifestation of cyclic variations in flame development. Measurements were conducted across a wide range of equivalence ratios ($0.2 \leq \phi_{H_2} \leq 0.55$ and $0.7 \leq \phi_{C_3H_8} \leq 1.5$) under comparable initial conditions to assess the projected flame characteristics for each mixture. In examining the pressure traces under identical conditions, some significant finding emerges. Figure 11 shows the in-cylinder pressure traces against the crank angle for three equivalence ratios for each fuel: 0.70, 1.00, and 1.50 for propane; and 0.25, 0.40, and 0.55 for hydrogen. It also highlights the five fastest (red) and slowest (blue) cycles in the initial 10% of fuel burned. These findings reveal that both lean and rich propane flames under the same conditions as ultra-lean hydrogen combustion exhibit different responses. Primarily, the in-cylinder pressure and combustion sensitivity to the equivalence ratio are much higher for propane than for hydrogen. In hydrogen-air mixtures, the discernible differences in pressure curves and the standard deviation of indicated mean effective pressures suggest that the flame is subject to less cycle-to-cycle variation than propane.

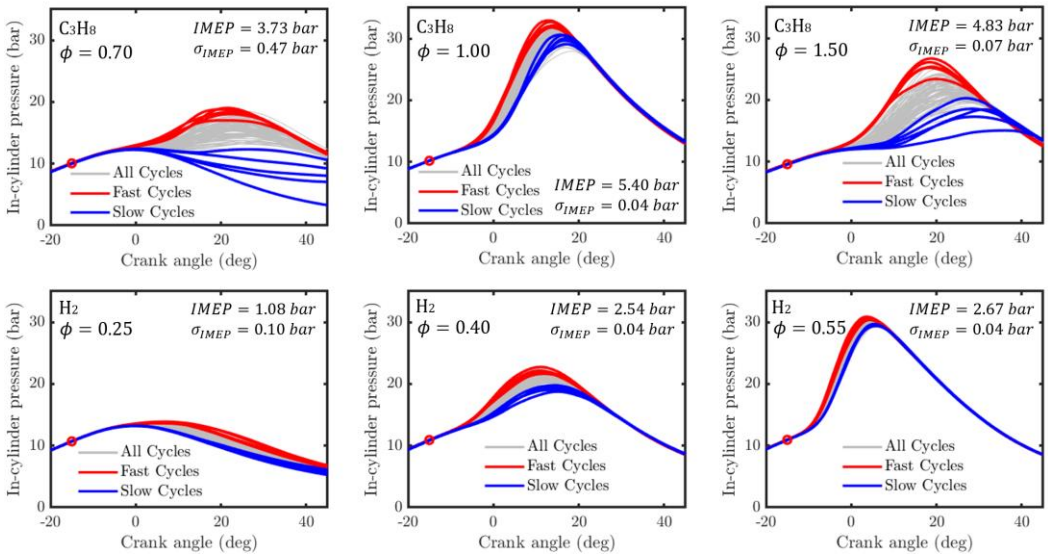

Figure. 11 In-cylinder pressure as a function of the crank angle for three equivalence ratios for each fuel. Fastest (red) and slowest (blue) cycles at 10% of mass fraction burned.

As depicted in Figure 12, flame development results indicate that the rate of radius growth increases with higher equivalence ratios for hydrogen. Furthermore, the standard deviations reveal that lower equivalence ratios exhibit greater cyclic variability, a trait typically associated with highly diluted and low flame speed mixtures (Truffin et al., 2015). In the case of propane, the highest flame

speeds are attained at equivalence ratios ranging between 1.0 and 1.1, consistent with laminar flame speed behavior. The standard deviations of equivalent flame speeds for both fuels are illustrated in Figures e) and f). It can be observed that the variations of propane flame speeds are notably lower, remaining under 1.5 m/s, compared to hydrogen, which exhibits variations of up to 3 m/s. This higher variation in flame development with hydrogen flames, combined with a lower variation in in-cylinder pressure, suggests that hydrogen flame velocity varies with the flow field. This variation in flame propagation results in a consistent increase in chamber pressure every cycle, thereby enhancing operational stability.

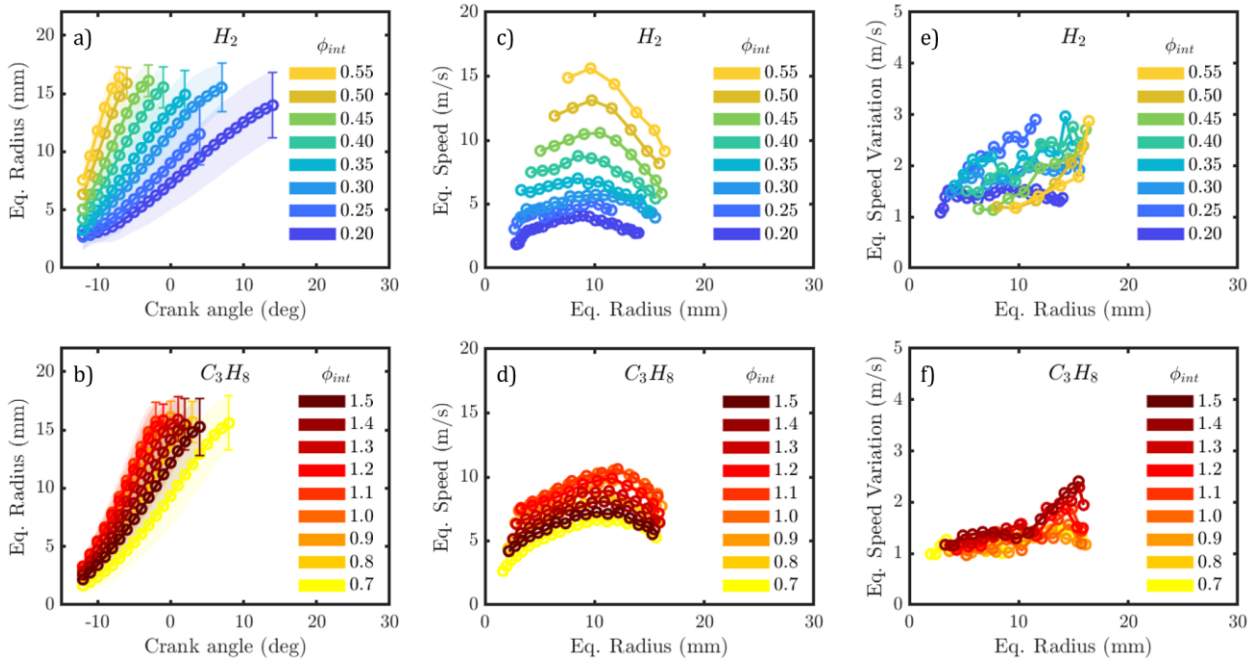

Figure. 12 Equivalent flame radius development as a function of the crank angle for (a) hydrogen and (b) propane at multiple equivalence ratios. Equivalent flame propagation speed as a function of the equivalent flame radius for (c) hydrogen and (d) propane. Equivalent propagation speed variability as a function of the flame radius for (e) hydrogen and (f) propane. The error bars are relative to $\pm 2\sigma$.

4. Fast and slow cycles characterization

In order to identify the differences in flame variability, the chemiluminescence images of the five fastest and slowest cycles under the most variable propane condition are depicted in Figure 13. It's notable that the slower cycles, as identified from the in-cylinder pressure traces, exhibit slower flame development. Moreover, this delayed development persists across all measurable domains

(i.e., from -14 to 10 °aTDC). As previously mentioned, the in-cylinder pressure trace correlates directly with flame development with higher in-cylinder pressures being caused by faster early flame development, as illustrated in Figure 9b. Lastly, the centroid of the fastest flames exhibits a displacement towards the center of the combustion chamber (at y = -5 mm). In contrast, the slower flames primarily propagate in the x direction, pushing them toward the cylinder walls sooner than the faster flames.

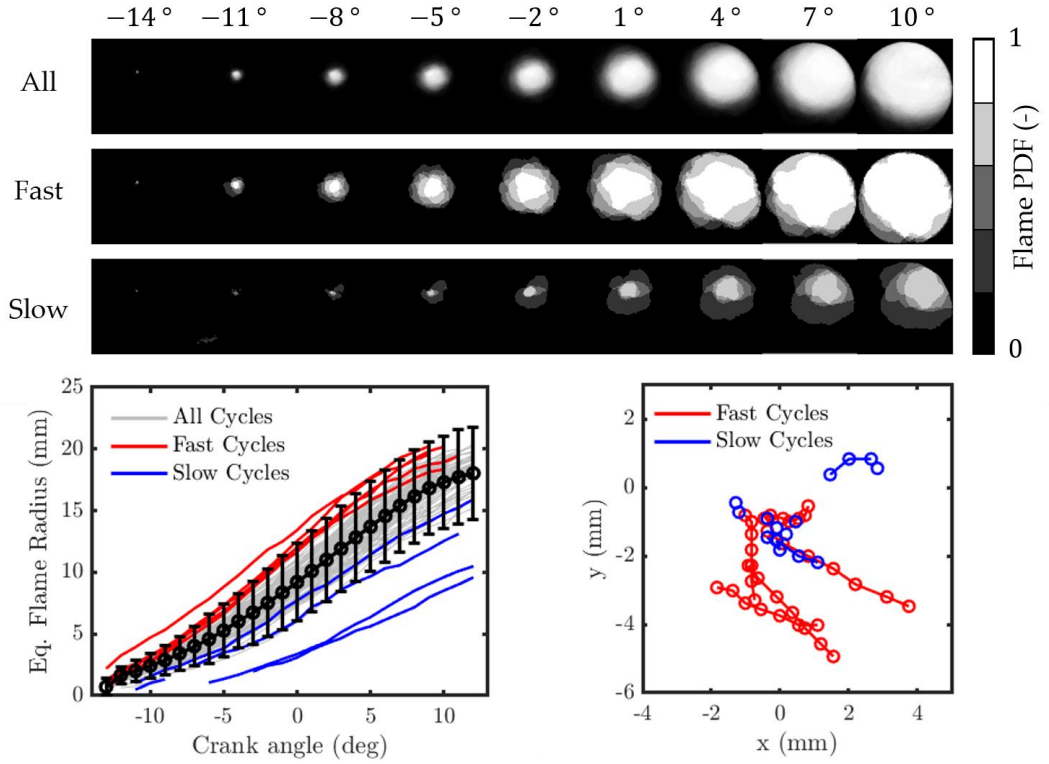

Figure. 13 Flame pdf of 5 fastest and slowest cycles for propane at an equivalence ratio of 0.70. Flame equivalent radius as a function of the crank angle and centroid pathways. The error bars are relative to $\pm 2\sigma$.

A similar analysis was conducted with hydrogen-air flames exhibiting the highest IMEP variation, meaning the most unstable condition regarding engine operation, i.e. with an equivalence ratio of 0.25. This analysis is displayed in Figure 14. The faster and slower cycles, as identified by the cylinder pressure analysis, also display correspondingly faster and slower flame radius development, respectively. However, unlike propane, the paths of the fastest flames appear to originate further from the spark plug, a phenomenon also observed in the literature with conventional fuels which concludes that the flame develop faster away from the spark plug (Welch et al., 2023).

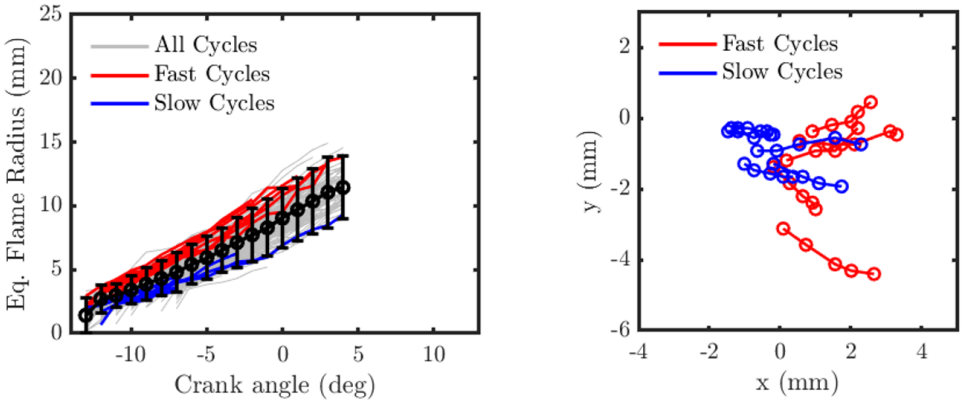

Figure. 14 Equivalent flame radius speed as a function of the crank angle and centroid paths for a hydrogen-air mixture of 0.25. The error bars are relative to $\pm 2\sigma$.

The engine's overall performance underscores a significant correlation between the in-cylinder pressure trace and flame radius development. To explore this correlation further, additional investigations were conducted to compare the relationship between flame patterns and specific aerodynamic structures present at the spark timing.

Simultaneous PIV and chemiluminescence measurements were conducted to observe the velocity fields present during the fast and slow cycles of hydrogen-air mixtures with an equivalence ratio of 0.4. The mean PIV for the five fastest and slowest cycles, along with their flame probability density functions (PDFs), are depicted in Figure 15. The PIV measurements reveal that the faster cycles tend to exhibit a stronger tumble with faster U velocities, both during mid-compression and near-spark timing crank angles, which agrees with the fast cycles flame centroid pathways that are advected further away from the spark plug, mainly at the ignition phase seen in Figure 14. This could be explained by the fact that the slower cycles present a less intense flow field upstream of the spark plug, which indicates that the flame remains in a zone with less turbulence at the ignition phase and its flame speed takes more time to be enhanced by the flow. In the fast cycles, however, the flame is advected to the more turbulent zone, seen in Figure 7, more rapidly,

The chemiluminescence images illustrate that the faster cycles generally display a faster flame overall. However, unlike propane, the hydrogen flames of the slower cycles resemble those of the faster cycles with a delay of 4 crank angle degrees. Upon closer examination of these flames with a 4 CAD interval, it becomes apparent that the development of the slower flames mirrors that of the faster flames. This suggests that while hydrogen flames may exhibit some variability in flame

kernel formation and early development, once the flame begins to develop from an equivalent radius of around 5 mm, the development remains consistent regardless of differences in the observed velocity fields. This was also observed in the literature, comparing the CCVs of H_2-air flames to gasoline (Kim et al., 2005). Finally, both the fast and slow cycle flames exhibited similar development within their respective groups, indicating that the hydrogen flame development has a generally well-defined trajectory and growth rate, differently from propane.

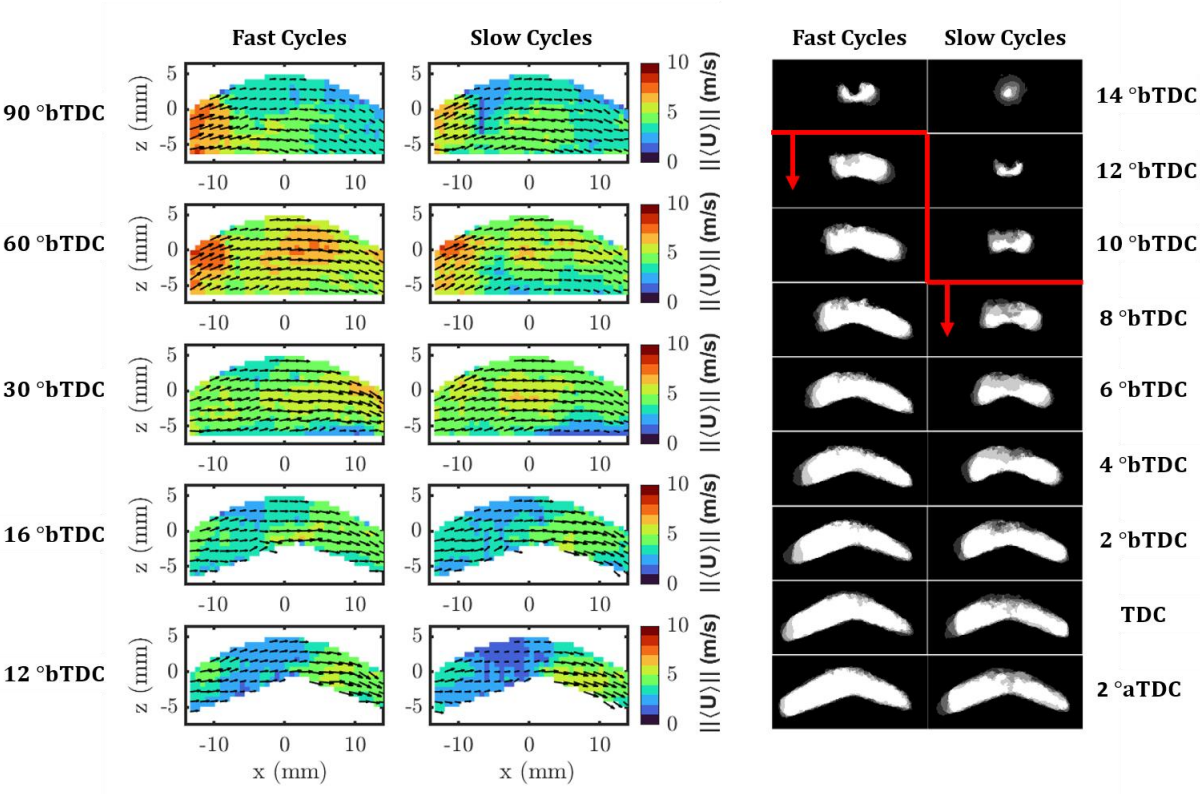

Figure. 15 Mean velocities fields for both fast and slow cycles for hydrogen-air mixtures with an equivalence ratio of 0.4 from 90 to 12 °bTDC (left) and chemiluminescence of the flames at these cycles from 15 °bTDC to 2 °aTDC (right). Red arrows: CAD where similar developments are seen.

4. Conclusions

In conclusion, this study offers insights into the combustion characteristics and cyclic variations of ultra-lean hydrogen-air flames compared to propane-air flames within an internal combustion engine. Key factors influencing combustion stability and flame behavior were investigated through a series of analyses, including in-cylinder pressure traces, Particle Image Velocimetry, and chemiluminescence imaging.

The findings underscored significant differences between hydrogen and propane combustion, particularly in response to varying equivalence ratios. Notably, while propane combustion exhibited higher sensitivity to deviations from stoichiometry, leading to increased cyclic variations and misfires, hydrogen combustion demonstrated greater robustness, showing less variability sensitivity to changes in equivalence ratio.

Chemiluminescence measurements provided further insights, revealing distinct flame characteristics between hydrogen and propane. Hydrogen flames exhibited faster growth rates with lower cyclic variability, particularly at higher equivalence ratios. Conversely, propane flames displayed more stable flame speeds across a range of equivalence ratios, with variations below those observed in hydrogen flames.

Additionally, PIV analysis elucidated the influence of aerodynamics on flame development and in-cylinder pressure variations. The results highlighted the correlation between in-cylinder flow patterns, flame propagation, and pressure fluctuations, further emphasizing the intricate interplay between combustion dynamics and aerodynamics.

Acknowledgments

The authors gratefully acknowledge the generous support of the Agence Nationale de Recherche under grant number 20-CE05-0007.

References

Berger, L., Attili, A., & Pitsch, H. (2022). Intrinsic instabilities in premixed hydrogen flames: parametric variation of pressure, equivalence ratio, and temperature. Part 2 – Non-linear regime and flame speed enhancement. *Combustion and Flame*, *240*. https://doi.org/10.1016/j.combustflame.2021.111936

Chu, H., Berger, L., Grenga, T., Gauding, M., Cai, L., & Pitsch, H. (2023). Effects of turbulence on variations in early development of hydrogen and iso-octane flame kernels under engine conditions. *Combustion and Flame*, *255*. https://doi.org/10.1016/j.combustflame.2023.112914

Chu, H., Berger, L., Grenga, T., Wu, Z., & Pitsch, H. (2023). Effects of differential diffusion on hydrogen flame kernel development under engine conditions. *Proceedings of the Combustion Institute*, *39*(2), 2129–2138. https://doi.org/10.1016/j.proci.2022.07.042

Ding, Z., Truffin, K., Jay, S., Schmidt, M., Foucher, F., & Borée, J. (2023). On the Use of LES and 3D Empirical Mode Decomposition for Analyzing Cycle-to-Cycle Variations of In-Cylinder Tumbling Flow. In *Flow, Turbulence and Combustion* (Vol. 111, Issue 1, pp. 235–284). Springer Science and Business Media B.V. https://doi.org/10.1007/s10494-023-00405-6

Enaux, B., Granet, V., Vermorel, O., Lacour, C., Pera, C., Angelberger, C., & Poinsot, T. (2011). LES study of cycle-to-cycle variations in a spark ignition engine. *Proceedings of the Combustion Institute*, *33*(2), 3115–3122. https://doi.org/10.1016/j.proci.2010.07.038

Kim, Y. Y., Lee, J. T., & Choi, G. H. (2005). An investigation on the causes of cycle variation in direct injection hydrogen fueled engines. *International Journal of Hydrogen Energy*, *30*(1), 69–76. https://doi.org/10.1016/j.ijhydene.2004.03.041

Lebrouhi, B. E., Djoupo, J. J., Lamrani, B., Benabdelaziz, K., & Kousksou, T. (2022). Global hydrogen development - A technological and geopolitical overview. In *International Journal of Hydrogen Energy* (Vol. 47, Issue 11, pp. 7016–7048). Elsevier Ltd. https://doi.org/10.1016/j.ijhydene.2021.12.076

Ramalho Leite, C., Laignel, M., Brequigny, P., Borée, J., & Foucher, F. (2023). Experimental Combustion Analysis in a Gasoline Baseline Hydrogen-Fueled Internal Combustion Engine at Ultra-Lean Conditions. *SAE Technical Papers*. https://doi.org/10.4271/2023-24-0073

Ramalho Leite, C., Oung, R., Brequigny, P., Borée, J., & Foucher, F. (2023, April 11). Combustion Cycle-To-Cycle Variation Analysis in Diesel Baseline Hydrogen-Fueled Spark-Ignition Engines. *SAE Technical Papers*. https://doi.org/10.4271/2023-01-0290

Sadeghi, M., Foucher, F., Abed-Meraim, K., & Mounaïm-Rousselle, C. (2019). Bivariate 2D empirical mode decomposition for analyzing instantaneous turbulent velocity field in unsteady flows. *Experiments in Fluids*, *60*(8). https://doi.org/10.1007/s00348-019-2775-5

Truffin, K., Angelberger, C., Richard, S., & Pera, C. (2015). Using large-eddy simulation and multivariate analysis to understand the sources of combustion cyclic variability in a spark-ignition engine. *Combustion and Flame*, *162*(12), 4371–4390. https://doi.org/10.1016/j.combustflame.2015.07.003

Verhelst, S., & Wallner, T. (2009). Hydrogen-fueled internal combustion engines. In *Progress in Energy and Combustion Science* (Vol. 35, Issue 6, pp. 490–527). https://doi.org/10.1016/j.pecs.2009.08.001

Welch, C., Schmidt, M., Illmann, L., Dreizler, A., & Böhm, B. (2023). The Influence of Flow on Cycle-to-Cycle Variations in a Spark-Ignition Engine: A Parametric Investigation of Increasing Exhaust Gas Recirculation Levels. *Flow, Turbulence and Combustion*, *110*(1), 185–208. https://doi.org/10.1007/s10494-022-00347-5